Article

New Insights on the Raman and SERS Spectra of Luteolin under Different Excitation Conditions: Experiments and DFT Calculations

Marilena Ricci [1], Emilio Mario Castellucci [2], Silvia Innocenti [3] and Maurizio Becucci [1,2,*]

[1] Department of Chemistry 'Ugo Schiff', University of Florence, Via della Lastruccia 3-13, 50019 Sesto Fiorentino, Italy
[2] European Laboratory for Non Linear Spectroscopy (LENS), University of Florence, Via N. Carrara 1, 50019 Sesto Fiorentino, Italy
[3] CNR-INO National Research Council, National Institute of Optics, Largo E. Fermi 6, 50125 Florence, Italy
[*] Correspondence: maurizio.becucci@unifi.it; Tel.: +39-0554573089

Abstract: We have studied, by density functional theory, the interaction between luteolin and Ag, devising two complexes where an Ag_{14} cluster faces two different sites of the molecule. The two sites are identified as quinoid-like and cathecol-like, and the complexes are CPLX1 and CPLX2, respectively. Raman and SERS spectra of luteolin were measured at different excitation wavelengths. Luteolin solid samples from different suppliers have different Raman spectra, possibly associated with different arrangements in the solids. These spectra are well reproduced by our DFT calculations. Assignment of the vibrational modes of luteolin and of the two luteolin–Ag_{14} complexes is obtained thanks to decomposition of the normal coordinates in terms of internal coordinates. The calculated Raman spectrum for CPLX1 seems to better reproduce the experimental SERS spectra. CPLX2 furnishes a spectrum still resembling that of luteolin in the high frequency region and is possibly responsible for some weak bands in the 1400–1700 cm^{-1} range that cannot be accounted by the CPLX1 system. SERS spectra are dependent on the Raman excitation wavelength. The calculation of the electronic spectrum suggests the presence of charge-transfer states, which might be responsible for the changes in the SERS spectra.

Keywords: flavonoid; luteolin; Raman; SERS; Ag-clusters; DFT

1. Introduction

Flavonoids are natural phenolic compounds ubiquitous in plants and, therefore, found in a variety of herbs, vegetables and fruits. Luteolin (5, 7, 3′, 4′-tetrahydroxyflavone) is one of the most common flavones, it is found in different plants (such as celery, green pepper and chamomile) and its most outstanding biological properties are its antioxidant, anti-inflammatory and antitumor activities [1–3]. Luteolin is also the main component of weld, a pigment derived by the leaves and stem of *Reseda luteola* L., which has been used in textile industries since ancient times as a mordent dye and is responsible for its characteristic yellow color [4,5]. Spectroscopic methods are used as analytical methods to identify the presence of flavonoids, even for in-field applications [6]. Recently, Surface Enhanced Raman Spectroscopy (SERS) was proposed as a sensitive and specific method for this purpose [7–9]. Its possible application for quantitative dye determination has been discussed [10]. This requires both the spectroscopic characterization of these systems and a detailed description of the molecule–substrate interaction [11].

The electronic and vibrational spectra of luteolin were studied in comparison with those of similar molecules chrysin, apigenin and quercetin [12]. The chemical and spectroscopic behavior of these molecules were strongly dependent on the number of OH groups in each molecule. Luteolin is rich in OH group content and, in addition, offers two distinct

sites for bidentate complexation with metals, identified by the groups $HOC_5/C_4=O$ and $HOC_{3'}/C_{4'}OH$ (Figure 1).
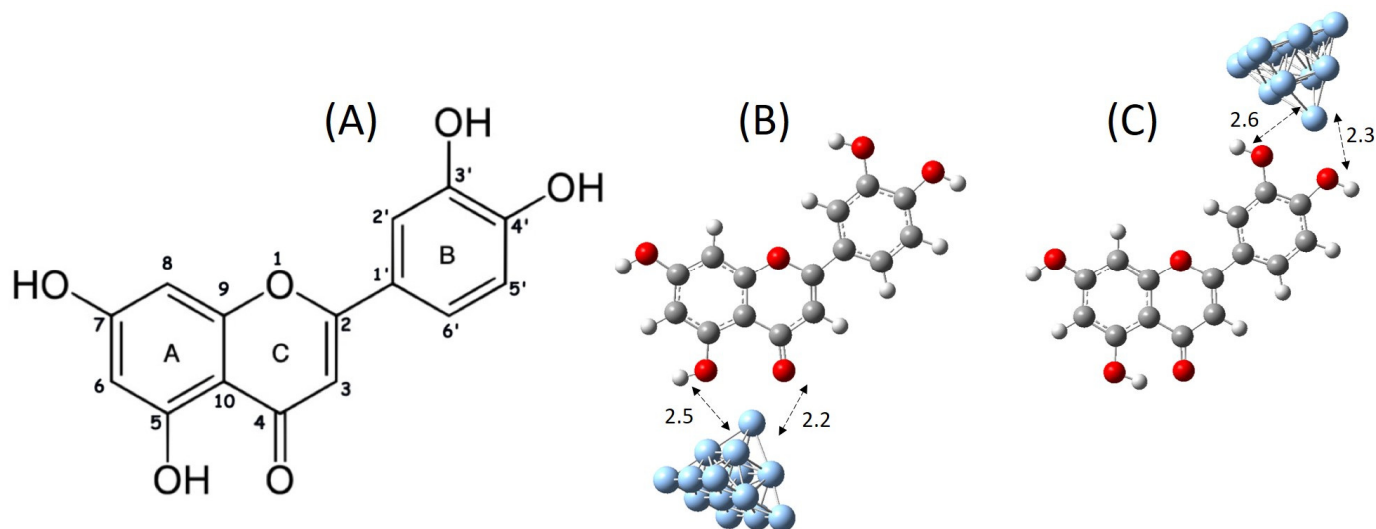

Figure 1. Atom and ring labeling for luteolin (**A**); optimized geometries (see text for details) for the two possible luteolin–Ag14 clusters we investigated: CPLX1 (**B**) and CPLX2 (**C**). The O–Ag distances (units Å) in the molecule to cluster main interaction points are shown.

Changes in electronic absorption spectra (red shift) after complexation were found for luteolin complexes with Al^{+3} [13,14]. Changes in the Raman frequency of modes of luteolin adsorbed on silver nanoparticles were also quoted in various papers [8,14–16]. SERS spectra of luteolin on silver colloid showed a negative shift of the strong line at 1608 cm^{-1} in solid to 1577 cm^{-1}. This was explained by the effect of polymerization of the catechol-like moiety on the Ag nanoparticles [12].

Other observations on the spectral behavior of luteolin adsorbed over colloid Ag nanoparticles (SERS spectra) dealt with the enhancement of the in-plane modes of the molecule with respect to the out-of-plane modes [16]. There are important frequency changes around 1600 cm^{-1}, i.e., the 1612 cm^{-1} results weaken and the line at 1576 cm^{-1} shifts to 1582 cm^{-1} and is the strongest line in the colloid spectrum. The spectral range is that of the C=O and C=C stretching. Furthermore, the lines at 1220 cm^{-1} and 1502 cm^{-1} are strongly enhanced relative to nearby lines. The lines at 468, 509 and 596 cm^{-1} are also considerably enhanced by proximity to the surface.

The observation of important changes in the SERS spectra of the adsorbed molecule with respect to the Raman spectrum of the bare molecule prompted the set-up of hypotheses on the adsorption geometry [12]. A simulation of the adsorption of luteolin on the colloid nanoparticles is then in order. Moreover, a detailed analysis of the calculated vibrational spectra of luteolin should shed light on the spectral changes occurring when the molecule is adsorbed on colloid.

Different Ag clusters have been reported in the recent literature to furnish a valid metal-molecule structure for an adequate simulation of the scattering terms contributing to the SERS spectra. In addition, the vertex of the cluster well-represents binding to an adatom site [17–21]. With the help of ab initio and DFT calculation, the electronic, Raman and IR spectra of the molecule and the complex can be calculated, and, afterwards, a comparison can be carried out on the experimental spectra [22]. By adopting a sufficiently accurate level of theory and an appropriate basis set of functions, a DFT calculation can provide a realistic reproduction of the spectra [20,23]. Then, the assignment of the vibrational modes of luteolin, free and in a complex with a silver cluster, can be made. We simulate here the adsorption on colloid through the interaction of the molecule with an Ag$_{14}$ cluster in the shape of a pyramid.

According to Refs. [24,25], for molecules adsorbed on a metal surface, the scattering intensity of the SERS spectrum should depend on four mechanisms: (1) ground state interaction between the molecule and the Ag cluster and resonance of the excitation with (2) surface plasmon levels, (3) charge-transfer levels and (4) internal energy levels. Far from resonances, only the ground state interaction mechanism should be operative in the determination of the spectrum of the complex. Then, the calculated static Raman spectra of the bare molecule and of the complex should be better compared with the Raman and SERS spectra obtained with excitation far from any resonance.

In SERS, however, the ground state interaction mechanism cannot be separated completely from the other enhancement mechanisms. In particular, the resonance with charge transfer levels, which are often found while the molecule–metal interaction takes place, has to be taken into account [19]. As the plasmonic and the internal energy resonance maxima occur for luteolin below 450 nm, for excitations at 514, 785 and 1064 nm, only ground state and, if present, charge-transfer enhancement mechanisms should be acting. We proceeded then to a TD-DFT calculation of the energy levels of the complexes in order to support this hypothesis.

The results of the calculation of the static Raman spectra, both of the free and the complexed molecule, will help to figure out the geometry of adsorption on the surface, either through the cathecol-like moiety on ring B or the quinoid C=O/OH group on rings C and A. Furthermore, the assignment of the SERS spectra with respect to model calculations can provide a deeper insight on the system.

2. Experimental Section

2.1. Materials and Sample Preparation for SERS Experiments

Luteolin was purchased from Selleck (>99% purity, measured by 1H-NMR and LC-MS) and Sigma-Aldrich (>98% purity, determined by TLC method).

Silver nanoparticles (hereafter: AgNPs or Ag colloid) were prepared either by synthesis or laser ablation methods. AgNPs synthesis followed the standard Lee–Meisel method, starting from silver nitrate (50 mL, 10^{-3} M in H_2O) and using sodium citrate (1 mL, 3.4×10^{-2} M in H_2O) as a reducing agent [26]. The resulting AgNPs were characterized by UV–vis spectra. Extinction spectra were measured on sample solutions held in a 1-mm optical path quartz cuvette. The plasmonic band maximum of the AgNPs' dispersion was found around 418 nm (indicating an average diameter of about 45 nm) with an FWHM of ~100 nm. In addition, we prepared AgNPs by laser ablation of a silver target (Aldrich, 0.5-mm thickness, 99.9% purity) in deionized water using the fundamental emission of a Q-switched Nd:YAG laser (Quanta System G90-10: 1064 nm, repetition rate 10 Hz, pulse width 10 ns). The laser pulse energy was set at 20 mJ/pulse (200 mW) with a laser spot of approximately 1-mm diameter and corresponding fluence of 2.5 J/cm^2. The target plate was fixed at the bottom of a glass vessel filled with ~6 mL of liquid [27]. The AgNPs obtained with ns pulses exhibited a bimodal size distribution, the one corresponding to small NPs was centered at 2–3 nm, while the other peaked at 17 nm.

Raman spectra were measured with a dye solution in ethanol of 10^{-2} M.

The SERS spectra in bulk solution were acquired at a 10^{-5} M concentration. The samples were prepared by adding 300 μL of water to 600 μL of colloidal dispersion in a 1-cm optical path length quartz cuvette, continuously stirred with a small magnetic bar. Afterwards, 100 μL of 10^{-4} M dye solution in ethanol was added, followed by addition of 3 μL of 1 M KNO$_3$ in water to induce nanoparticle aggregation. In the background spectrum, the dye solution was substituted by ethanol. The measurements were collected after 10 min from sample preparation. This time delay between the sample preparation and the measure of the SERS spectrum was chosen, after a few initial tests, in order to have good signals and reproducible conditions.

SERS spectra were measured also with a microRaman setup on small drops at 10^{-5} M luteolin concentration. The samples were obtained by adding, in order, the AgNPs, the KNO$_3$ solution, 0.5 M, only in the case of Lee–Meisel colloid use, and the dye solution (in

ethanol) in a proportion of 2:1:1. SERS measurements were performed by focusing the laser beam on a small drop (4 μL) of the dye–colloid system deposited on the surface of an aluminium foil.

The pH of solution prepared for SERS experiments was in the 6–6.5 range, depending on the preparation of the AgNPs. Given the reported values for the acidic dissociation constants for luteolin in methanol–water solutions, in our samples, luteolin is expected to be in its neutral form [28].

The Raman and SERS spectra, either for samples in solution or solid, were obtained by exciting with different laser wavelengths and spectrometers, as described in the following section.

2.2. Instruments

Raman and SERS spectra of luteolin solution were recorded using a Raman spectrometer based on an Acton SP150 monochromator, equipped with 600 lines/mm or 1200 lines/mm holographic gratings, and a Princeton Instruments Pixis CCD detector thermoelectrically cooled. Different solid-state lasers were aligned to the spectrometer and holographic notch filters (OD 4–6) were used for rejection of the elastically scattered radiation. We used 457 and 532 nm laser excitations and the full 200–4000 cm^{-1} spectrum was measured in a single acquisition on the CCD camera with the 1200 and 600 lines/mm grating. The spectral resolution (FWHM of narrow bands) was around 10 cm^{-1}. Typical laser power on the sample was about 10 mW to avoid instabilities in the colloid. The colloidal dispersion stability was checked by the measurement of its Uv–vis spectrum before and after Raman measurements. As a further precaution, the laser beam was blocked when measurements were not running. Typical acquisition times for Raman and SERS experiments were 10–30 s and the spectra were measured 5–10 times to verify the experiment reproducibility and, in case, averaged to improve the quality of the results.

In the case of Raman measurements under 1064 nm laser excitation, a Bruker Multi-RAM FT-Raman spectrometer was used, setting the resolution to 4 cm^{-1} for each acquisition. Raman measurements were performed using the same ethanol solution used in the experiments described above. After an initial check for sample stability, the laser power used was 350 or 150 mW for Raman and SERS experiments, respectively. Signals were averaged for 1000 scans.

All the spectra were normalized by laser power and integration time. Furthermore, we have verified that ethanol can act as an internal standard, allowing a reliable comparison between frequencies and intensities of the spectra excited at various wavelengths. In this case, the intensity is normalized with respect to the intensity of the line at 882 cm^{-1} of ethanol as an internal standard.

The Raman spectra of solid luteolin and the SERS spectra of the luteolin solution (drops) were recorded with a Renishaw single-grating (1200 grooves/mm) RM2000 micro-Raman spectrometer and a charge-coupled device (CCD) air-cooled (577 × 400 pixels) detector, employing 514 or 785 nm as excitation laser lines. The 20x objective of the Leica microscope was used for both excitation and signal collection in Raman and SERS measurements. Spectra were measured with a spectral resolution of 4 cm^{-1}.

For the Raman spectra of the solid, the laser power on the sample was 2 mW in the case of 785 nm excitation and 20 μW in the case of 514 nm excitation, with an integration time of 10 s for 10 averages. For SERS measurements, a laser power of about 1 mW and 200 μW, respectively, for 785 nm and 514 nm excitation wavelengths was used, and the integration time was 10 s.

2.3. Computational Methods

Ground-state geometry optimization and Raman spectra were calculated for luteolin and luteolin–Ag_{14} complexes using the suite of programs Gaussian 16 [29].

The atom numbering and ring labeling of the three rings for luteolin is shown in Figure 1. If luteolin is exposed to a metal surface, it presents two different sites, which

should be prone to adsorption by the metal, i.e., C(4)=O/C(5)-OH on rings C and A, and C(3′)-OH/C(4′)-OH on ring B.

The SERS active substrate was modeled as an Ag_{14} cluster, assuming a cubic T_d structure corresponding to the *fcc* structure of the elementary cell of the Ag crystal lattice. Its structure was optimized and not subject to further refinement in the following calculations.

We optimized the luteolin–Ag_{14} complex starting from different initial arrangements of the two moieties, where the Ag_{14} cluster faces either one or the other molecular site, and the optimizations come out with the two conformations shown in Figure 1. Along the text, we indicate these complexes as CPLX1 and CPLX2. The resulting geometries are also mimicking the edge-on set-up of the molecule on the surface. The spectral features of the two geometries of adsorption should be different, such that conclusions about the geometry of adsorption could be drawn after a careful study of the details of the vibrational and electronic spectra of the bare molecule and of the molecule adsorbed on the metal surface.

With this respect, the study of the population of the normal mode coordinate in terms of redundant internal coordinates, as obtained from the DFT frequency calculation, has been of great help.

The luteolin–Ag_{14} complexes are left to adjust their geometry to a minimum of the energy surface with the Ag_{14} cluster being completely frozen in its previously optimized geometry. The final geometry can be accepted as a structural minimum of the potential surface, as all six eternal modes have negligible frequency, only one being slightly negative. The optimized structures of CPLX1 and CPLX2 complexes are reported in Figure 1.

The basis set for the atoms, except Ag, was the 6–31 + g(d,p). For silver atoms, the valence electrons and internal shells were described employing the ECP basis LANL2DZ. The B3LYP hybrid functional was used, as it is known to provide a good accuracy in the calculation of frequency-dependent polarizabilities and Raman scattering activity [17,30,31].

The calculated spectra were given a Lorentzian FWHM of 6 cm^{-1}, and a scaling factor of 0.97 was applied to the calculated wavenumbers such that a good match of frequencies with the experimental ones was obtained for the luteolin molecule. Indeed, previous work suggested the use of a double frequency scaling factor for better agreement between calculated and experimental data, but we prefer not to over-parametrize our model [16].

Calculated Raman spectra are possibly reported either as Raman activities (Å^4/amu unit) or scattering cross-section units (cm^2/sr). As shown by Placzek's polarizability theory, Raman intensities should be calculated with frequency-dependent polarizability derivatives [32]. For polyatomics, the important quantities are the derivatives of the polarizability tensor components with respect to normal coordinates. In fact, the Raman activity S (Å^4/amu units), which is defined as

$$S_k = \left(45\alpha_k^{'2} + 7\gamma_k^{'2} \right)$$

is calculated for each vibrational normal mode k. Here, α' and γ' are the derivatives of the polarizability invariants (where k label in the formula refers to the vibrational mode), i.e., the mean polarizability and the anisotropic polarizability, respectively. With observation perpendicular to the linearly polarized incoming laser beam, the expression for Differential Raman Scattering Cross-Section (DRSCS), with units 10^{-30} cm^2/sr, is

$$I_{Raman}^k = (2\pi)^4 \, (\nu_{in} - \nu_k)^4 \, \frac{h}{8\pi^2 c \nu_k} \, \frac{S_k}{45} \, \frac{1}{[1 - exp(hc\nu_k/K_B T)]}$$

In the equation, besides the well-known universal constants, ν_{in} and ν_k are the frequencies, in cm^{-1}, of the incident light and of the k_{th} vibrational mode. S_k is the Raman activity, which is directly obtained by the DFT calculation. The formula is valid within the double harmonic approximation, which assumes harmonic vibrational wavefunctions and uses only the first derivatives of the polarizability with respect to nuclear displacement. The static polarizability Raman spectra of both luteolin and its complexes with the Ag_{14} cluster were computed to investigate the effects (frequency shifts and changes of intensity)

of the ground-state interaction between the molecule and the silver cluster. In addition, pre-resonance Raman spectra of luteolin were calculated at the excitation wavelengths used in the experiments.

3. Results and Discussion

3.1. Raman Spectroscopy of Luteolin

We have measured Raman spectra of luteolin (powder) as obtained from the two suppliers and, quite surprisingly, we have obtained different results, as shown in Figure 2. The Raman spectra measured on samples from Sigma-Aldrich (sample 1) compare quite well with those reported in previous work, while those from materials obtained from Selleck (sample 2) are significantly different [16]. The corresponding Raman spectra measured in ethanol 10^{-2} M solution were identical for both samples, and a representative spectrum is provided in the Supplementary Information (Figure S1).
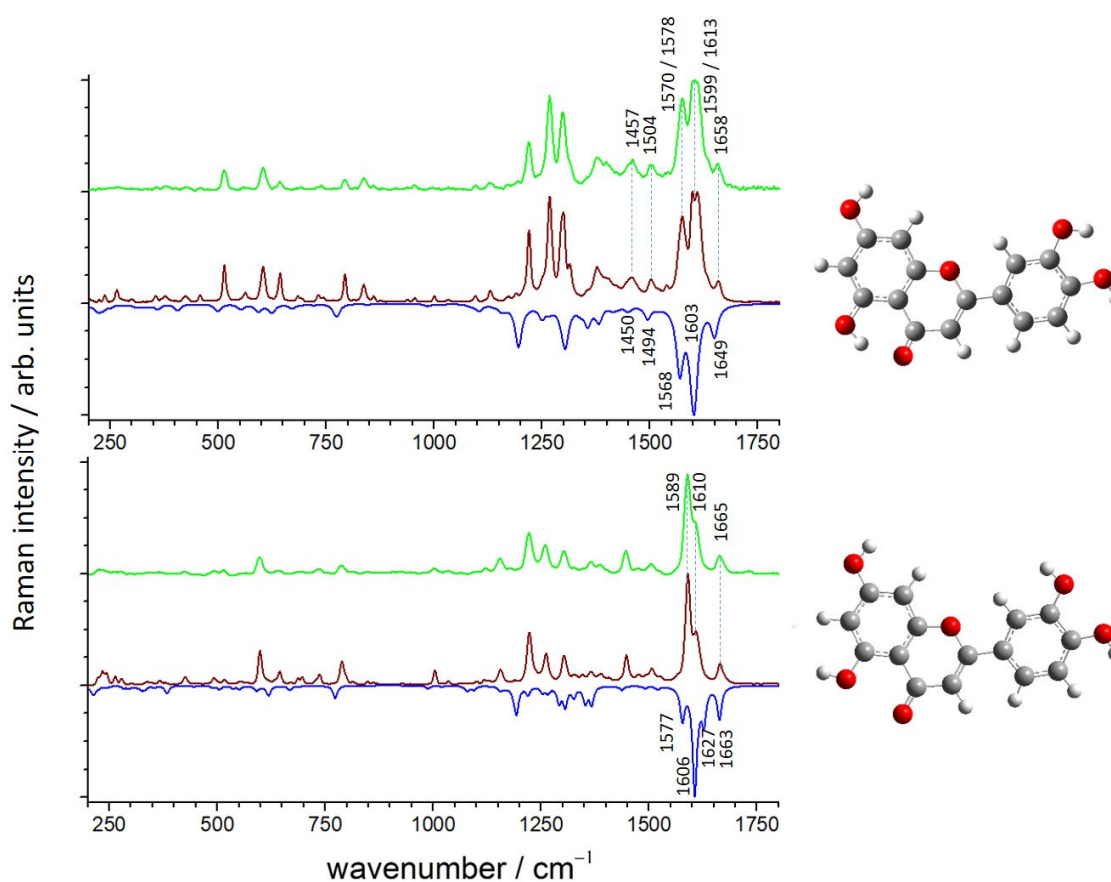

Figure 2. Experimental Raman spectra of luteolin powder from different suppliers: sample 1 from Sigma-Aldrich (upper panel) and sample 2 from Selleck (lower panel) measured with 514 and 785 nm excitation (top and middle trace, respectively) compared to calculated Raman spectra (DRSCS for 785 nm excitation, bottom reverse trace) of isolated luteolin molecules in different conformations. Some relevant bands discussed along the text are marked.

We were able to obtain computational results in good agreement with experimental data by assuming a possible different orientation of the OH group at the C(5) atom corresponding to the possible formation of an intramolecular H-bond. Therefore, given the stated purity grade of the samples that rules out the possible presence of relevant chemical impurities, we assume that, in the solid state, more than one crystal structure exists for luteolin. The Raman spectrum from the Sigma-Aldrich sample fully corresponds to that calculated from a luteolin molecule in the geometry reported by Cox et al. from an X-ray diffraction study [33].

In addition, we have extended our Raman spectroscopy data to verify if pre-resonance Raman effects are possibly relevant for luteolin under visible or near-infrared excitation. We have measured the Raman spectrum of both samples under different excitation conditions (from 457 to 1064 nm excitation) and no major spectral changes were observed (see Figure 2). The calculated pre-resonance Raman spectra are in good agreement with the experimental evidence, as shown in Supplementary Information Figure S2.

Our results demonstrate that the local interactions at the C(4)=O/C(5)-OH on rings C and A play a major role in the 1500–1700 cm^{-1} part of the spectrum. In the Supplementary Information (Tables S1 and S2), we summarize the assignment for the more evident Raman bands of both samples based on DFT calculations. In the spectral region of the C=O stretching mode, 1600–1700 cm^{-1}, the Raman spectra of the two samples differ considerably. Sample 2 shows a series of bands at higher frequency with respect to sample 1. This is associated, according to our model, with the possible formation of an intramolecular hydrogen bond in sample 1 that leads to a larger coupling between the C(4)=O group and the C(5)-OH group. According to our calculations, the C=O stretching mode shows a single relevant contribution to the *77* mode (1663 cm^{-1}) for the open conformer (sample 2). Instead, in the hydrogen-bonded conformer, the C=O stretching mode contributes similarly to the *77* (1649 cm^{-1}), *75* (1603 cm^{-1}) and *69* (1450 cm^{-1}) modes, where it is coupled to the C(5)-OH bending mode, among others. The two OH groups in the B ring are more relevant for the description of vibrations in the spectral region below 1350 cm^{-1} for both conformers. Our assignment based on the hydrogen-bonded conformer for sample 1 spectra agrees quite well with previous work [16].

3.2. SERS Spectroscopy of Luteolin and its DFT Modeling

We measured luteolin SERS spectra using as active substrate the Ag nanoparticles obtained either by chemical reduction of Ag$^+$ ions in solution (Lee–Meisel method) or by laser ablation of an Ag metal plate [26,27]. The first method is commonly used in SERS spectroscopy but can suffer from the interaction of reactants/reaction products from synthesis to the surface of the AgNPs. The second method, more demanding in terms of experimental resources, allows for the synthesis of AgNPs with a virtually clean surface (apart for possible oxidation). The comparison of SERS spectra obtained with the two methods will allow us to assess the relevance of possible chemical impurities in the stabilization of the luteolin–AgNPs adducts and to possibly evidence the presence of other reaction products.

The luteolin SERS spectra were calculated by using the DFT method and evaluating the Raman spectrum of luteolin–Ag$_{14}$ clusters in different conformations, as shown in Figure 1, for the two more relevant geometries.

In the case of CPLX1, the Ag$_{14}$ cluster directly interacts with oxygen atoms on rings A and C (C4=O/C5-OH), breaking the possible intramolecular hydrogen bond and leading to a non-planar geometry. In the case of the CPLX2 cluster, where the Ag cluster binds to the luteolin cathecol group in ring B, our calculation converges to a conformation where the intramolecular hydrogen bond in the A–C rings exists. From our calculations, it comes out that CPLX2 is slightly more stable (less than 0.01 Hartree) than CPLX1. The difference could be possibly ascribed to the intramolecular H-bond present in CPLX2. However, additional interactions of the different OH groups with protic solvents could possibly revert the stability order for the two complexes in solution. Our calculations show that at least two oxygen atoms of luteolin are at a distance from the Ag cluster below 3 Å (see Figure 1), suggesting the relevance of the chemical contribution to the SERS enhancement mechanism and supporting the choice of a rather large Ag cluster, such as Ag$_{14}$, to model the luteolin–AgNPs interaction.

In Figure 3, we show the experimental luteolin SERS spectra obtained with the laser-ablated Ag colloid for 785 and 514 nm excitation and the calculated Raman spectra for different luteolin–Ag$_{14}$ clusters.
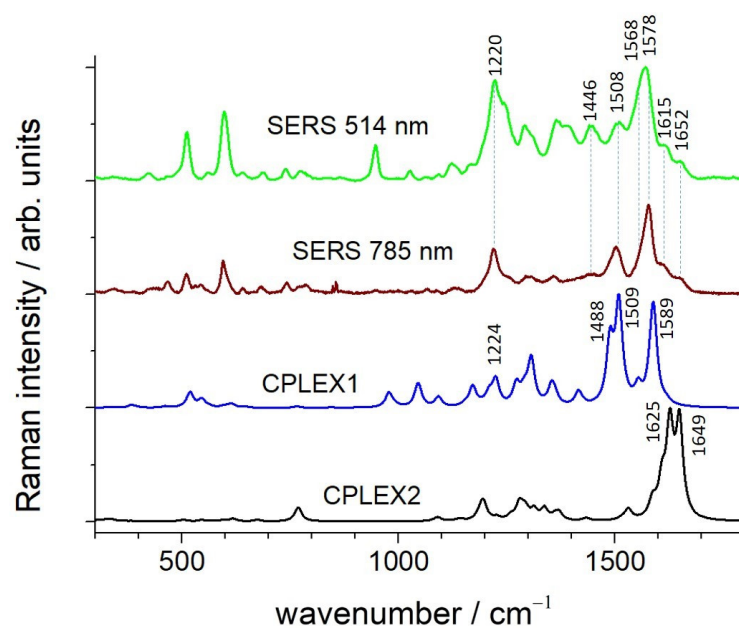
Figure 3. Experimental SERS spectra of luteolin (785 and 514 nm excitation, laser-ablated AgNPs in a drop with luteolin 10^{-5} M on aluminum film) and calculated SERS spectra of luteolin (DRSCS) for the CPLX1 and CPLX2 models. Some relevant bands discussed along the text are marked.

The calculated Raman spectrum of CPLX2, a complex that is bound by interactions involving the C3′-OH and C4′-OH groups on the B ring, exhibits, in the higher frequency region, 1600–1800 cm^{-1}, the same bands as luteolin (see Figures 2 (left panel) and 3) and does not reproduce the significant red shift observed in the SERS spectra. Instead, this down-shift of the high frequency pattern of bands observed in experimental SERS spectra is well reproduced by the calculated CPLX1 spectrum, a system bound by interactions involving the C4=O/C5-OH groups. It is worth noticing that the free luteolin data already show this trend when the C=O group is affected by secondary interactions, such as the intramolecular H-bond. Furthermore, in the CPLX1 case, other features of the experimental SERS spectrum are quite well reproduced. The pattern of calculated bands between 1600 and 1570 cm^{-1} for CPLX1 is able to reproduce the large, very strong feature of the SERS spectrum ~1580 cm^{-1}. The other strong band at 1502 cm^{-1} is reasonably shown in the calculated spectrum, even if with much higher intensity, and has a large C=O character. The strong line at 1220 cm^{-1} is only partially reproduced by the calculations and is assigned to CCH bendings in the A and B rings. The SERS pattern between 420 and 620 cm^{-1} is also in part reproduced. Therefore, the calculated Raman spectrum of the neutral CPLX1 points in the right direction in terms of frequency shifts. However, the medium intensity bands above 1600 cm^{-1} in the SERS spectra cannot be accounted for by the calculated Raman spectrum for CPLX1. These bands are a distinctive signature of the "free" C=O stretching, which could possibly be found only in different cluster conformations, such as that represented by CPLX2. In conclusion, we believe that the most statistically representative conformation of the luteolin–Ag_{14} complex is represented by CPLX1, but the existence of different conformers, represented by CPLX2, must be taken into account for a full description of the experimental results. Indeed, theoretical calculations point to a similar stability for the two conformers.

An extended comparison between the vibrational properties of free luteolin (with or without intramolecular hydrogen bonds) and its complexes with Ag clusters (CPLX1 and CPLX2), described in terms of internal coordinates, is provided in the Supplementary Information (Tables S1–S4). The main results are discussed here, taking as a reference the isolated luteolin molecule in structure A, which provides a Raman spectrum more similar to the one observed in EtOH/water solutions.

The most characteristic strong and isolated bands either in the Raman or SERS spectra of luteolin are in the 1660–1500 cm^{-1} region. The luteolin band at 1658 cm^{-1} (assigned as the 1649 cm^{-1} mode in our calculations, mostly localized on the rings A and C with some C=O stretching character) does not find a clear correspondence in the CPLX1-calculated Raman spectrum, while it corresponds in Raman shift and character to the mode calculated at 1649 cm^{-1} for CPLX2 (the strongest band in its spectrum) and shows up as a medium/weak shoulder in the luteolin SERS spectrum at approx. 1650 cm^{-1}. Similarly, the bands at 1613 and 1599 cm^{-1} in luteolin (assigned to modes involving ring B and C=O stretching and calculated at 1603 and 1596 cm^{-1}) do not find a good correspondence in the CPLX1 spectrum, while they correspond to similar vibrational modes of CPLX2 (calculated at 1625 and 1610 cm^{-1}) and show up as a medium/weak band at 1612 cm^{-1} in the luteolin SERS spectrum. Instead, the strong luteolin band at 1575 cm^{-1}, assigned to C=C stretching on rings A and C coupled to CCH bending on ring C, finds a good correspondence in the CPLX1 bands at 1578 and 1569 cm^{-1} (which conserve the same character as in free luteolin), and together they are the strongest feature in the luteolin SERS spectrum. The strong bands at 1509 and 1446 cm^{-1} in the luteolin SERS spectrum, based on our calculations, are assigned to CC stretching and bending (either CCH or COH) on rings A and C strongly coupled to C=O stretching. It is quite good evidence of the chemical interaction between luteolin and the Ag$_{14}$ cluster that lowers significantly the force constant (and therefore the vibrational frequency) of C=O stretching. It should be noticed that previous work [2] was not able to account for the 1502 cm^{-1} strong band in the SERS spectrum.

In summary, changes of the normal modes character are calculated for CPLX1 internal coordinates involving groups of atoms located on rings A and C, facing the Ag$_{14}$ cluster, in agreement with the local supramolecular interaction between the two units. This is observed for both in-plane modes (stretching and bending) and out-of-plane modes. However, if the weight of the C=O on ring C (corresponding to the C=O stretching coordinate) changes a lot, this does not occur for the OH stretching coordinate on ring A, suggesting a lower interaction between this group and the metal cluster. No noticeable change in frequencies and intensity in the 1600–1800 cm^{-1} range of frequencies is, on the contrary, observed for the luteolin CPLX2 complex with respect to the free molecule (see Figure 3). This last complex exhibits instead an appreciable negative shift of frequencies in the range of 1200–1500 cm^{-1}, where the bending modes of the OH groups of ring B mainly occur.

In conclusion, the characteristic bands that show a marked C=O character are, in our opinion, the best indicator for the luteolin–Ag$_{14}$ complex conformation. Their analysis allows us to identify the conformer CPLX1, characterized by a strong C=O–Ag$_{14}$ interaction, as the most representative for the species responsible of the luteolin SERS spectrum. In addition, we have found evidence for the existence of a second conformer, identified as CPLX2, characterized by the interaction of the two O-H groups on luteolin ring B with the Ag$_{14}$ cluster. We are not able to give a reasonable quantitative estimation of the population of the two conformers given the large errors inherent the Raman cross-sections calculation of the two species. Based on an intensity fit on the bands in the 1680–1500 cm^{-1} spectral region in the SERS spectrum of luteolin, the CPLX2 conformer accounts for about 20% of the observed signals.

3.3. Charge-Transfer Effects in the SERS Spectra of Luteolin

We have registered the luteolin SERS spectrum at different excitation wavelengths and with different plasmonic nanoparticles. In Figure 4, we show the plasmonic extinction band of the different AgNPs used, obtained by laser ablation of chemical reduction of Ag$^+$ ions, together with markers at the different excitation wavelengths used for our experiments (1064 nm excitation not shown). The wavelength of the peak extinction band is a measure of the AgNPs average dimensions, and the bandwidth of the peak is proportional to the size dispersion. Therefore, from our data, it is clear that the AgNPs obtained by laser ablation are smaller in diameter and quite uniform in dimensions, while those from synthesis are

larger and produced in a wider set of dimensions. In both cases, the wavelength of laser excitation for the SERS experiments is larger than the absorption maximum.
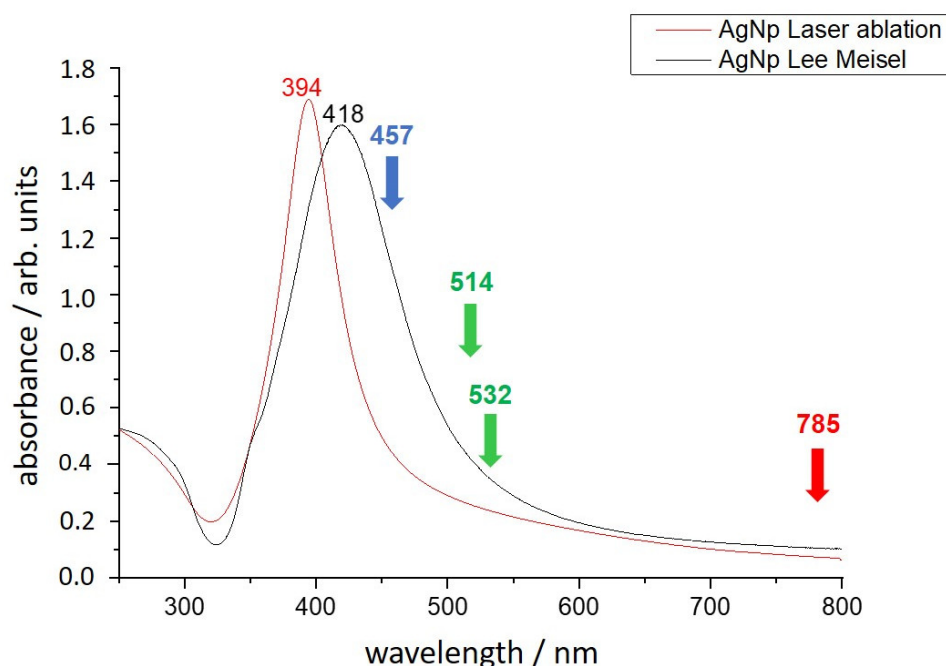

Figure 4. The absorption spectrum of the AgNPs used in our SERS experiments (red line data for AgNPs from laser ablation, black line from chemical synthesis). For reference, the excitation wavelengths used in Raman/SERS experiments are marked (1064 nm excitation not shown).

According to the theory of Raman and SERS processes, we should expect a larger cross-section for excitation at shorter wavelengths and closer to the peak absorption of the AgNPs. Quite surprisingly, the luteolin SERS spectra do not follow an ordinary trend. The observed enhancement factor for 532 nm excitation is larger than for 457 nm excitation, and the intensity pattern of the SERS bands is clearly excitation wavelength-dependent. In order to shed some light on this result, it is important to remember that the luteolin Raman spectrum in solution does not show resonance effects under excitation at different wavelengths in the visible range (see Figure 2).

The SERS spectra measured in solution, either on a drop in the microRaman setup (AgNPs from laser ablation) or in the macro Raman setup in a cuvette (AgNPs from synthesis), are shown in Figure 5.

Spectra obtained with different SERS substrates (laser-ablated or from synthesis) do not show significant changes. Instead, SERS spectra obtained with different laser excitation wavelengths show marked differences, both in terms of relative intensity and spectral shape. The SERS spectrum measured at 785 nm, with respect to those measured with blue-green excitation, has a low global intensity in the range of 1250–1450 cm^{-1} and a prominent peak at 1502 cm^{-1}. The SERs spectrum measured with 1064 nm excitation has an overall shape intermediated between the two previous cases. This evidence points to some electronic resonance effects in the SERS spectra of the luteolin–Ag$_{14}$ complex. Another possible signature for this effect can be found by looking at the dependence of the SERS enhancement factor with respect to the excitation wavelength.

The analytical enhancement factor (AEF) was determined for SERS spectra measured in bulk as

$$AEF = \frac{I^{SERS} \times C^{Raman}}{I^{Raman} \times C^{SERS}}$$

where the averaged intensities of the SERS and Raman spectra (I^{SERS} and I^{Raman}) and the analytical luteolin concentration in the samples (C^{SERS} and C^{Raman}) are included [34,35].
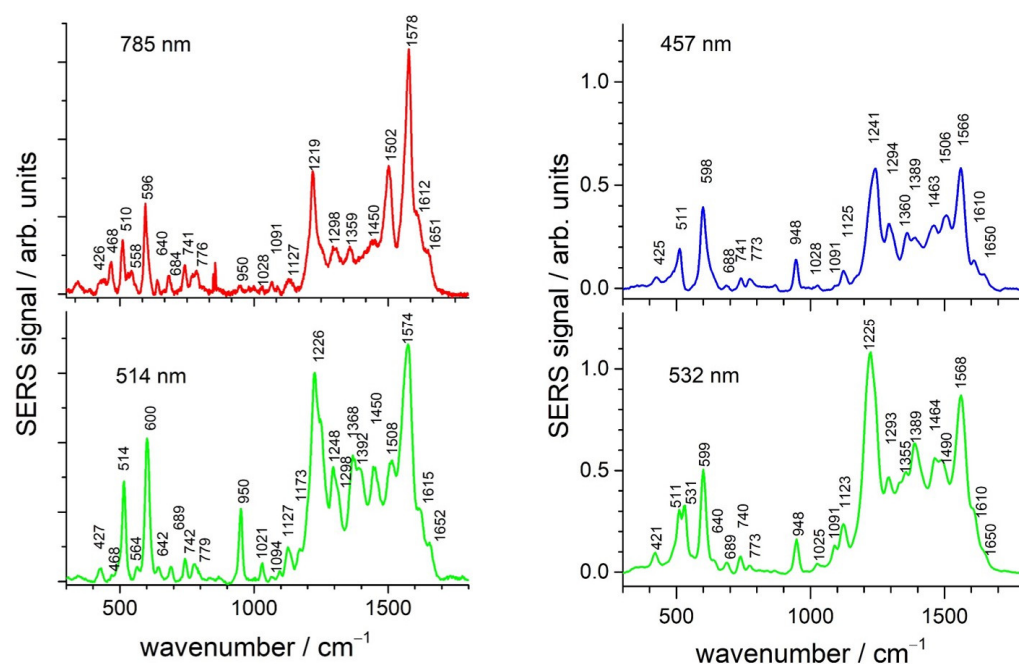
Figure 5. SERS spectrum of luteolin 10^{-5} M in ethanol. Left panel: laser-ablated AgNPs, sample in a drop under the microscope objective, signals normalized to the major peak at ~1575 cm^{-1}. Right panel: chemically-synthesized AgNPs, sample in a quartz cuvette, signals normalized on the 882 cm^{-1} main peak of ethanol before blank signal subtraction.

While it is quite difficult to have a reliable reference signal for intensity normalization purposes working in the microRaman setup, when operating on samples in a quartz cuvette, the solvent can provide convenient Raman signal that allows us to normalize the SERS spectra intensities to a common reference. Therefore, to have a good reproducibility and accuracy, the intensity of the Raman/SERS spectra obtained from samples in a cuvette are normalized on the main ethanol Raman band at 882 cm^{-1} before blank signal subtraction. The resulting spectra are shown in Figure S3. Then, we determine the Raman/SERS signal intensity by averaging the intensities of the measured signals in the 400–1800 cm^{-1} spectral range. As a result, we have determined a larger average analytical enhancement factor in the SERS signal measured with 532 nm and 457 nm excitation with respect to those measured for 1064 nm excitation, with values of 6×10^4, 3×10^4 and 2×10^3, respectively.

This evidence points to a relevant contribution of photoinduced charge-transfer metal↔molecule transitions to the enhancement of the luteolin SERS spectrum. The role of intramolecular excitations is ruled out by the measurement of the luteolin electronic absorption spectrum (which exhibits a maximum in the near UV at 352 nm in ethanol and no other resonances in the visible range) and by the independence of the measured luteolin Raman spectrum in both in solid and solution with respect to the excitation wavelength (shown in Figures 2 and S3, left).

To corroborate this hypothesis, we calculated the electronic spectrum of the luteolin–Ag$_{14}$ model systems by using the TD-DFT approach (same level of theory as previously described) including the first 80 electronic singlet transitions. Many Ag$_{14}$ intra-cluster electronic transitions and some charge-transfer transitions are predicted in the relevant spectral range (400–1000 nm) with non-negligible intensity. In Figure 6, we show the calculated UV–Vis spectra for luteolin and the luteolin–Ag$_{14}$ clusters (red arrows point to the intramolecular electronic transition in the luteolin system, while blue arrows point to the transitions with a larger charge-transfer character, according to the molecular orbitals more involved in their description—details in Tables S5 and S6). Examples of the relevant molecular orbitals involved in these transitions are also shown in Figure 6. An alternative view can be provided by the analysis of the Natural Bond Orbitals [36,37]. The present results on the electronic properties of these complexes, even if not quantitatively correct,

provide a quite solid background for the interpretation of the experimental results and strongly support the evidence of a relevant role of charge-transfer transitions in the SERS spectrum of luteolin. A quantitative agreement would be possible only if a much more realistic model for the Ag clusters is developed and the correct level of theory for resonance Raman calculations is applied. At present, we find it difficult to proceed any further in this direction due to the crude description of the AgNPs as an Ag_{14} pyramidal cluster.
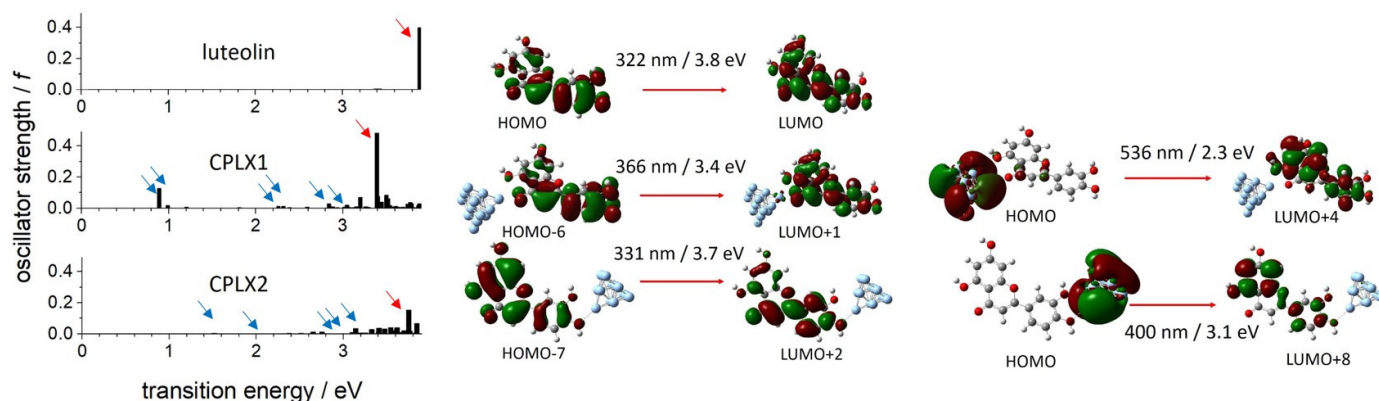

Figure 6. Calculated electronic spectrum (left panel) for luteolin and its complexes formed with Ag_{14} clusters, CPLX1 and CPLX2: the red arrows point to the lowest allowed electronic transition localized in the luteolin frame and the blue arrows point to charge-transfer transition between the luteolin frame and the Ag14 cluster. The molecular orbitals involved in the lowest allowed electronic transition localized in the luteolin frame for the different systems are shown in the central panel. Molecular orbitals involved in representative charge-transfer transitions for the luteolin–Ag_{14} CPLX1 and CPLX2 complexes are shown in the right panel.

In detail, from our calculations, we find that the near UV-allowed electronic transition of luteolin is described as arising from two allowed electronic transitions (at 353 (weak) and 322 ($f = 0.40$) nm; experimental value 348 nm in water and 352 nm in ethanol), in agreement with previous computational work, while, in CPLX1 and CPLX2, the lowest intramolecular electronic transition, similar to the HOMO-LUMO luteolin transition, is calculated at 366 ($f = 0.48$) and 331 ($f = 0.15$) nm, respectively [38]. A large difference for the intramolecular electronic transition for the different complex conformations was already reported for the luteolin–Al^{3+} complexes [13].

4. Conclusions

Luteolin, among other flavon molecules, presents two possible sites of interaction with the surface of nanoparticles of silver colloids. One site is of cathecol-type, C3′-OH/C4′-OH on ring B, and the other of quinoid-type, i.e., C4=O/C5-OH on rings C and A (see Figure 1). The direct exposure of either group can occur only with the molecule arranged in an edge-on geometry (perpendicular) to the surface. The spectral response of either structures should be different, and, in turn, the thorough analysis of the Raman spectra can furnish solid hints about the geometry of adsorption.

It has been stressed by many authors that the adsorption of a molecule on a nanoparticle surface can be safely simulated by a complex formed by the molecule interacting with a small cluster of Ag atoms. In particular, in contrast to dielectric models, the cluster model of molecule–metal interfacial complexes can provide some key insights into the chemical bonding interaction and the charge-transfer mechanism in SERS processes. The time-dependent density functional theory (TD-DFT) method has been used to calculate the optical and vibrational spectra of the molecule and the complex and to suggest the dependence of SERS spectra on the incident wavelengths.

In the present report, we designed two possible structures able to simulate the interaction of luteolin and silver nanoparticle, devising a cluster of Ag_{14} facing either the quinoid- or cathecol-type molecular site. The two complexes are indicated as CPLX1 and CPLX2,

respectively. The assignment of the calculated frequencies of the Raman spectra of the two complexes to the corresponding frequencies of free luteolin has been obtained by careful inspection of the mode composition in term of internal coordinates. By a careful analysis of the bands involving the C=O stretching, it is possible to demonstrate that the more likely interaction of the AgNPs with the luteolin frame is on the quinoid side.

The experimental evidence and model calculations point to the relevance of the charge-transfer mechanism in the efficiency of the SERS process. Limits in the description of the Ag_n cluster and the low symmetry of the system do not allow for a detailed analysis of the charge-transfer SERS enhancement mechanism, e.g., following the relevance of the different Albrecht's terms for the efficiency of the Raman scattering process.

The present results show how the SERS spectrum is possibly sensitive to the geometry of the complex formed with the substrate and to experimental conditions in use, i.e., the excitation wavelength. Therefore, any attempt to identify flavonoid dyes by SERS methods must follow well-characterized procedures in order to possibly differentiate molecules with much similar chemical structure.

Supplementary Materials: The following supporting information can be downloaded at: https://www.mdpi.com/article/10.3390/chemosensors11020104/s1, Table S1: Raman spectrum of luteolin, sample 1 (from Sigma Aldrich): experimental data and proposed assignment based on DFT calculations on the hydrogen bonded conformer (Figure 2, left panel). Table S2: Raman spectrum of luteolin, sample 2 (from Selleck): experimental data and the proposed assignment based on DFT calculations (geometry shown in Figure 2, right panel). Table S3: SERS spectrum of luteolin: experimental data and the proposed assignment based on DFT calculations for the CPLX1 conformer. Table S4: SERS spectrum of luteolin: experimental data and the proposed assignment based on DFT calculations for the CPLX2 conformer. Table S5: Relevant charge transfer transitions in the near IR-visible spectrum of the luteolin-Ag_{14} CPLX1. Table S6: Relevant charge transfer transitions in the near IR- visible spectrum of the luteolin-Ag_{14} CPLX2. Figure S1: Raman spectrum of luteolin in ethanol (457 nm excitation), as obtained either from Sigma-Aldrich or Selleck suppliers. Figure S2: Pre-resonance Raman spectra (DRSCS, frequency unscaled) of luteolin calculated for relevant excitation wavelengths. Figure S3: Raman and SERS spectrum of luteolin in solution at different excitation wavelengths.

Author Contributions: Conceptualization, M.R., E.M.C. and M.B.; methodology, M.R., E.M.C. and M.B.; validation, M.R. and M.B.; investigation, M.R., S.I., E.M.C. and M.B.; resources, M.R. and M.B.; data curation, M.R., S.I., E.M.C. and M.B.; writing—original draft preparation, E.M.C.; writing—review and editing, M.R., E.M.C. and M.B.; visualization, M.R. and M.B. All authors have read and agreed to the published version of the manuscript.

Institutional Review Board Statement: Not applicable.

Informed Consent Statement: Not applicable.

Data Availability Statement: Data are available upon request to the authors.

Conflicts of Interest: The authors declare no conflict of interest.

References

1. Pandey, K.B.; Rizvi, S.I. Plant Polyphenols as Dietary Antioxidants in Human Health and Disease. *Oxid. Med. Cell. Longev.* **2009**, *2*, 270–278. [CrossRef] [PubMed]
2. Scarano, A.; Chieppa, M.; Santino, A. Looking at Flavonoid Biodiversity in Horticultural Crops: A Colored Mine with Nutritional Benefits. *Plants* **2018**, *7*, 98. [CrossRef]
3. Kopustinskiene, D.M.; Jakstas, V.; Savickas, A.; Bernatoniene, J. Flavonoids as Anticancer Agents. *Nutrure* **2020**, *12*, 457. [CrossRef] [PubMed]
4. Joosten, I.; Van Bommel, M.R.; De Keijzer, R.H.; Reschreiter, H. Micro analysis on hallstatt textiles: Colour and condition. *Microchim. Acta* **2006**, *155*, 169–174. [CrossRef]

5. Ferreira, E.S.B.; Hulme, A.N.; McNab, H.; Quye, A. The natural constituents of historical textile dyes. *Chem. Soc. Rev.* **2004**, *33*, 329–336. [CrossRef] [PubMed]

6. Ramos, R.; Bezerra, I.; Ferreira, M.; Soares, L. Spectrophotometric Quantification of Flavonoids in Herbal Material, Crude Extract, and Fractions from Leaves of Eugenia uniflora Linn. *Pharmacogn. Res.* **2017**, *9*, 253. [CrossRef]

7. Jurasekova, Z.; Domingo, C.; Garcia-Ramos, J.V.; Sanchez-Cortes, S. In situ detection of flavonoids in weld-dyed wool and silk textiles by surface-enhanced Raman scattering. *J. Raman Spectrosc.* **2008**, *39*, 1309–1312. [CrossRef]

8. Leona, M.; Stenger, J.; Ferloni, E. Application of surface-enhanced Raman scattering techniques to the ultrasensitive identification of natural dyes in works of art. *J. Raman Spectrosc.* **2006**, *37*, 981–992. [CrossRef]

9. Choi, J.M.; Hahm, E.; Park, K.; Jeong, D.; Rho, W.Y.; Kim, J.; Jeong, D.H.; Lee, Y.S.; Jhang, S.H.; Chung, H.J.; et al. SERS-based flavonoid detection using ethylenediamine-β-cyclodextrin as a capturing ligand. *Nanomaterials* **2017**, *7*, 8. [CrossRef]

10. Ricci, M.; Trombetta, E.; Castellucci, E.; Becucci, M. On the SERS quantitative determination of organic dyes. *J. Raman Spectrosc.* **2018**, *49*, 997–1005. [CrossRef]

11. Jurasekova, Z.; Marconi, G.; Sanchez-Cortes, S.; Torreggiani, A. Spectroscopic and molecular modeling studies on the binding of the flavonoid luteolin and human serum albumin. *Biopolymers* **2009**, *91*, 917–927. [CrossRef] [PubMed]

12. Jurasekova, Z.; Domingo, C.; Garcia-Ramos, J.V.; Sanchez-Cortes, S. Adsorption and catalysis of flavonoid quercetin on different plasmonic metal nanoparticles monitored by SERS. *J. Raman Spectrosc.* **2012**, *43*, 1913–1919. [CrossRef]

13. Amat, A.; Clementi, C.; Miliani, C.; Romani, A.; Sgamellotti, A.; Fantacci, S. Complexation of apigenin and luteolin in weld lake: A DFT/TDDFT investigation. *Phys. Chem. Chem. Phys.* **2010**, *12*, 6672–6684. [CrossRef] [PubMed]

14. Rygula, A.; Wrobel, T.P.; Szklarzewicz, J.; Baranska, M. Raman and UV-vis spectroscopy studies on luteolin-Al(III) complexes. *Vib. Spectrosc.* **2013**, *64*, 21–26. [CrossRef]

15. Bruni, S.; Guglielmi, V.; Pozzi, F. Historical organic dyes: A surface-enhanced Raman scattering (SERS) spectral database on Ag Lee-Meisel colloids aggregated by NaClO4. *J. Raman Spectrosc.* **2011**, *42*, 1267–1281. [CrossRef]

16. Corredor, C.; Teslova, T.; Cañamares, M.V.; Chen, Z.; Zhang, J.; Lombardi, J.R.; Leona, M. Raman and surface-enhanced Raman spectra of chrysin, apigenin and luteolin. *Vib. Spectrosc.* **2009**, *49*, 190–195. [CrossRef]

17. Zhao, L.; Jensen, L.; Schatz, G.C. Pyridine-Ag20 cluster: A model system for studying surface-enhanced Raman scattering. *J. Am. Chem. Soc.* **2006**, *128*, 2911–2919. [CrossRef]

18. Wu, D.Y.; Liu, X.M.; Duan, S.; Xu, X.; Ren, B.; Lin, S.H.; Tian, Z.Q. Chemical enhancement effects in SERS spectra: A quantum chemical study of pyridine interacting with copper, silver, gold and platinum metals. *J. Phys. Chem. C* **2008**, *112*, 4195–4204. [CrossRef]

19. Birke, R.L.; Lombardi, J.R.; Saidi, W.A.; Norman, P. Surface-Enhanced Raman Scattering Due to Charge-Transfer Resonances: A Time-Dependent Density Functional Theory Study of Ag13-4-Mercaptopyridine. *J. Phys. Chem. C* **2016**, *120*, 20721–20735. [CrossRef]

20. Lofrumento, C.; Platania, E.; Ricci, M.; Becucci, M.; Castellucci, E.M. SERS Spectra of Alizarin Anion–Ag n (n = 2, 4, 14) Systems: TDDFT Calculation and Comparison with Experiment. *J. Phys. Chem. C* **2016**, *120*, 12234–12241. [CrossRef]

21. Ricci, M.; Lofrumento, C.; Becucci, M.; Castellucci, E.M. The Raman and SERS spectra of indigo and indigo-Ag2 complex: DFT calculation and comparison with experiment. *Spectrochim. Acta. A. Mol. Biomol. Spectrosc.* **2017**, *188*, 141–148. [CrossRef] [PubMed]

22. van Trang, N.; Dao, D.Q.; Nhat, P.V.; Thuy, P.T.; Nguyen, M.T. A Cluster Model for Interpretation of Surface-Enhanced Raman Scattering of Organic Compounds Interacting with Silver Nanoparticles. In *Practical Aspects of Computational Chemistry V*; Springer: Cham, Switzerland, 2022; pp. 255–285. [CrossRef]

23. Van Dyck, C.; Fu, B.; Van Duyne, R.P.; Schatz, G.C.; Ratner, M.A. Deducing the Adsorption Geometry of Rhodamine 6G from the Surface-Induced Mode Renormalization in Surface-Enhanced Raman Spectroscopy. *J. Phys. Chem. C* **2018**, *122*, 465–473. [CrossRef]

24. Jensen, L.; Zhao, L.L.; Schatz, G.C. Size-dependence of the enhanced Raman scattering of pyridine adsorbed on Agn (n = 2–8, 20) clusters. *J. Phys. Chem. C* **2007**, *111*, 4756–4764. [CrossRef]

25. Lombardi, J.R.; Birke, R.L. A unified approach to surface-enhanced raman spectroscopy. *J. Phys. Chem. C* **2008**, *112*, 5605–5617. [CrossRef]

26. Lee, P.C.; Meisel, D. Adsorption and surface-enhanced Raman of dyes on silver and gold sols. *J. Phys. Chem.* **1982**, *86*, 3391–3395. [CrossRef]

27. Giorgetti, E.; Marsili, P.; Giammanco, F.; Trigari, S.; Gellini, C.; Muniz-Miranda, M. Ag nanoparticles obtained by pulsed laser ablation in water: Surface properties and SERS activity. *J. Raman Spectrosc.* **2015**, *46*, 462–469. [CrossRef]

28. Favaro, G.; Clementi, C.; Romani, A.; Vickackaite, V. Acidichromism and Ionochromism of Luteolin and Apigenin, the Main Components of the Naturally Occurring Yellow Weld: A Spectrophotometric and Fluorimetric Study. *J. Fluoresc.* **2016**, *17*, 707–714. [CrossRef]

29. Frisch, M.J.; Trucks, G.W.; Schlegel, H.B.; Scuseria, G.E.; Robb, M.A.; Cheeseman, J.R.; Scalmani, G.; Barone, V.; Petersson, G.A.; Nakatsuji, H.; et al. *Gaussian 16, Revision B.01*; Gaussian, Inc.: Wallingford, CT, USA, 2016.

30. Tirado-Rives, J.; Jorgensen, W.L. Performance of B3LYP density functional methods for a large set of organic molecules. *J. Chem. Theory Comput.* **2008**, *4*, 297–306. [CrossRef]

31. Lofrumento, C.; Arci, F.; Carlesi, S.; Ricci, M.; Castellucci, E.; Becucci, M. Safranin-O dye in the ground state. A study by density functional theory, Raman, SERS and infrared spectroscopy. *Spectrochim. Acta Part A Mol. Biomol. Spectrosc.* **2015**, *137*, 677–684. [CrossRef]
32. Albrecht, A.C. On the Theory of Raman Intensities. *J. Chem. Phys.* **1961**, *34*, 1476. [CrossRef]
33. Cox, P.J.; Kumarasamy, Y.; Nahar, L.; Sarker, S.D.; Shoeb, M. Luteolin. *Acta Crystallogr. Sect. E Struct. Rep.* **2003**, *59*, o975–o977. [CrossRef]
34. Le Ru, E.C.; Blackie, E.; Meyer, M.; Etchegoin, P.G. Surface Enhanced Raman Scattering Enhancement Factors: A Comprehensive Study. *J. Phys. Chem. C* **2007**, *111*, 13794–13803. [CrossRef]
35. Cañamares, M.V.; Garcia-Ramos, J.V.; Sanchez-Cortes, S.; Castillejo, M.; Oujja, M. Comparative SERS effectiveness of silver nanoparticles prepared by different methods: A study of the enhancement factor and the interfacial properties. *J. Colloid Interface Sci.* **2008**, *326*, 103–109. [CrossRef]
36. Buglak, A.A.; Kononov, A.I. Silver Cluster Interactions with Tyrosine: Towards Amino Acid Detection. *Int. J. Mol. Sci.* **2022**, *23*, 634. [CrossRef] [PubMed]
37. Weinhold, F.; Landis, C.R. Natural bond orbitals and extensions of localized bonding concepts. *Chem. Educ. Res. Pract.* **2001**, *2*, 91–104. [CrossRef]
38. Amat, A.; Dementia, C.; De Angelis, F.; Sgamellotti, A.; Fantacci, S. Absorption and emission of the apigenin and luteolin flavonoids: A TDDFT investigation. *J. Phys. Chem. A* **2009**, *113*, 15118–15126. [CrossRef]